Electronic Supplementary Material (ESI) for Chemical Science.

Supporting Information

Assessing the exchange coupling in binuclear lanthanide(III) complexes and the slow relaxation of the magnetization in the antiferromagnetically coupled Dy_2 derivative

Chun Y. Chow,[a] Hélène Bolvin,[b] Victoria E. Campbell,[c] Régis Guillot,[c] Jeff W. Kampf,[a] Wolfgang Wernsdorfer,[d], Frédéric Gendron[e], Jochen Autschbach[e], Vincent L. Pecoraro*[a] and Talal Mallah*[c]

[a]Department of Chemistry, University of Michigan, Ann Arbor, Michigan 48108-1005,
[b] Laboratiore de Chimie et Physique Quantiques, Université Toulouse III, 118 route de Narbonne, 31062 Toulouse, France
[c] Institut de Chimie Moléculaire et des Matériaux d'Orsay, CNRS, Université de Paris Sud 11, 91405 Orsay Cedex, France
[d]Institut Néel, CNRS, Université J. Fourier, BP 166 25, Avenue des Martyrs, 38405 Grenoble, France
[e]Department of Chemistry, University at Buffalo, State University of
New York, Buffalo, NY 14260-3000, USA

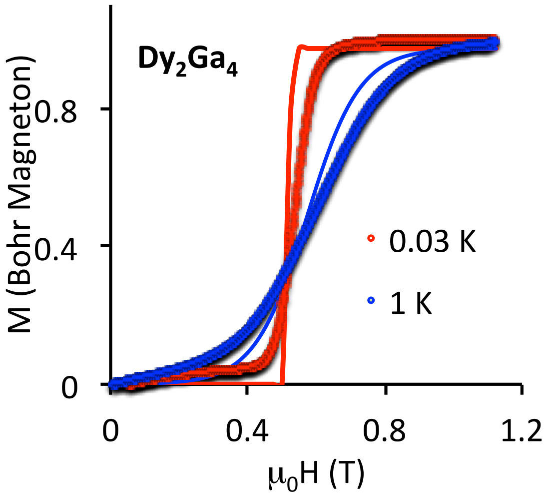

Figure S1. Magnetization *vs.* applied field at T = 1 and 0.03 K for complex **3**, with the crystal anisotropy axis parallel to the magnetic field. The solid lines correspond to the best fit (see text).

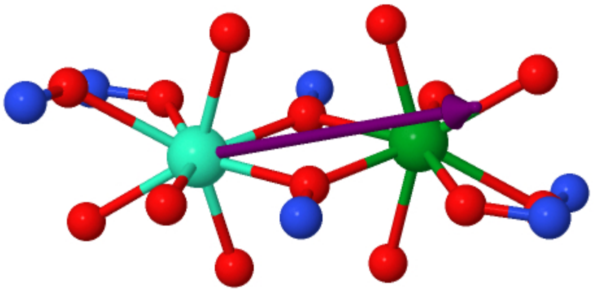

Figure S2. Orientation of the magnetization axis of the ground doublet $M_J = \pm 15/2$ of the Tb^{III} ion in **6** where one Tb^{III} has been replaced by a Lu^{III} ion.

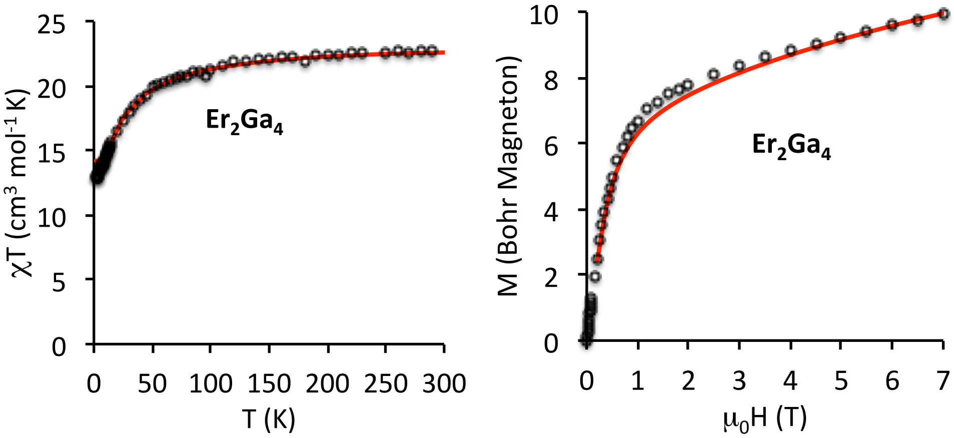

Figure S3. Temperature dependence of the χT product at 2000 Oe (left) and magnetization vs. applied field at 2 K for complex **5**. The solid lines correspond to the best fit (see text).

Calculation of the Natural Spin Orbitals (NSOs):

A local modification of MOLCAS was used to generate natural spin orbitals (NSOs) from SO-CASSCF calculations. Within the frame of the principal magnetic axes of the doublet ground state X, Y and Z, to generate the NSOs ϕ_p^u in direction $u = X, Y, Z$, one considers linear combinations of the ground state doublet components $\left|\Psi_0^u\right\rangle$ and $\left|\Psi_0'^u\right\rangle$ diagonalizing the magnetic moment operator $\widehat{M}_U$ and the NSOs ϕ_i^u are the eigen-functions of the one-particle spin-magnetization density matrices. It results that when the external magnetic field is applied along direction u, the spin density is $\rho^u(\boldsymbol{r}) = \sum_{i=1}^{7} n_i \phi_i(\boldsymbol{r})^2$ where ϕ_i is NSOi with occupation n_i. The spin magnetization in this direction is $\sum_{i=1}^{7} n_i = 2\langle \Psi_0^{\mathrm{u}} | \hat{S}_u | \Psi_0^{\mathrm{u}} \rangle = g_i^S/2$

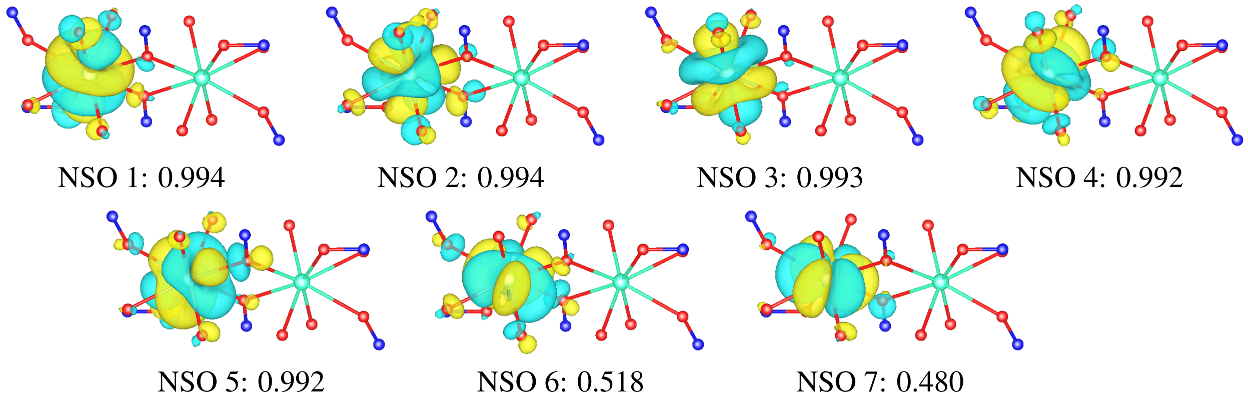

NSO 1: 0.994 NSO 2: 0.994 NSO 3: 0.993 NSO 4: 0.992

NSO 5: 0.992 NSO 6: 0.518 NSO 7: 0.480

Figure S4: NSOs for the Tb$^{\mathrm{III}}$ complex determined along the direction **1** corresponding to the orientation of the magnetization axis. One Tb$^{\mathrm{III}}$ has been replaced by a Lu$^{\mathrm{III}}$ ion. The isosurfaces are weighted by the corresponding occupation, which is indicated below each plot. The seven NSOs are close to the 4f orbitals with a quantization axis along direction **1** : NSO1 looks like a $4f_0$, NSO2 and NSO3 are the $4f_{\pm1}$, NSO4 and NSO5 $4f_{\pm2}$ and NSO6 and NSO7 $4f_{\pm3}$.

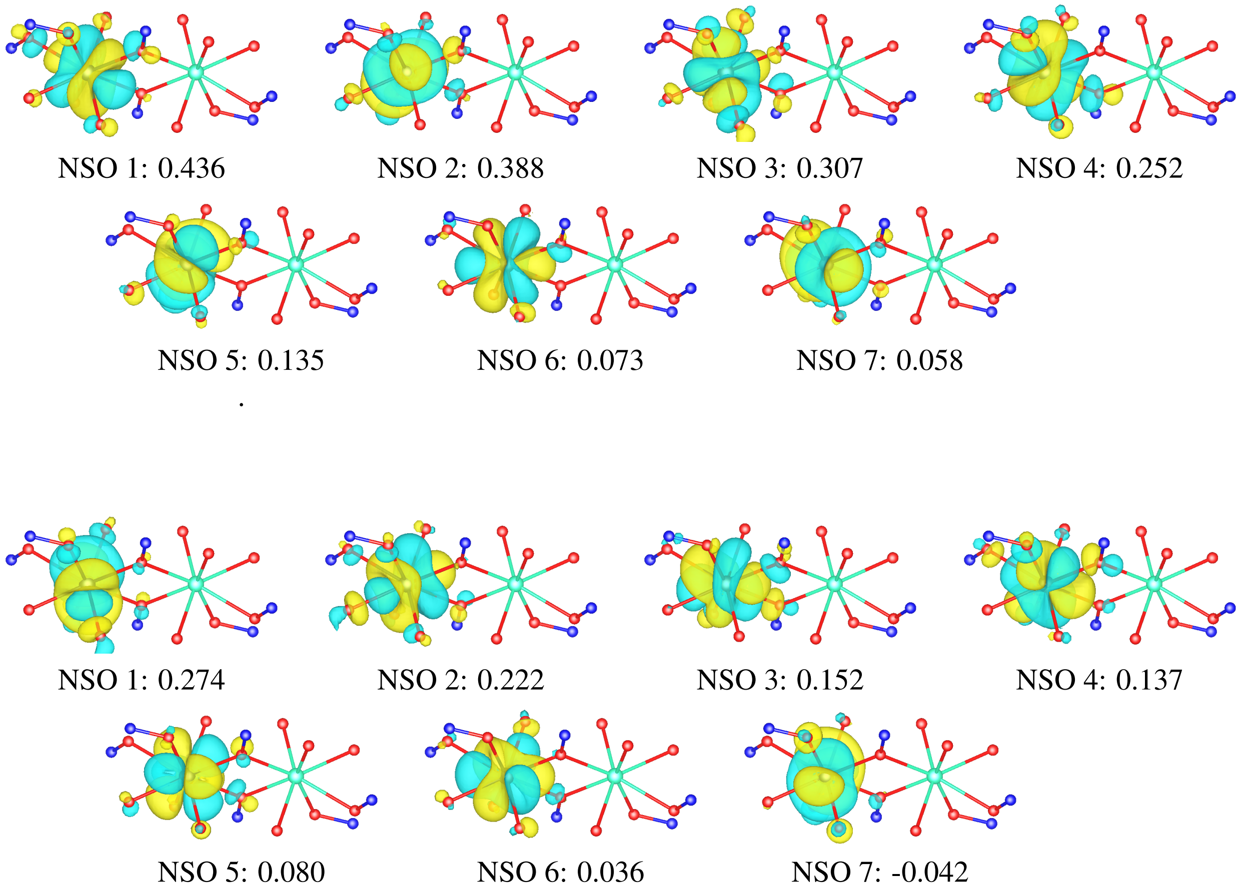

NSO 1: 0.436

NSO 2: 0.388

NSO 3: 0.307

NSO 4: 0.252

NSO 5: 0.135

NSO 6: 0.073

NSO 7: 0.058

NSO 1: 0.274

NSO 2: 0.222

NSO 3: 0.152

NSO 4: 0.137

NSO 5: 0.080

NSO 6: 0.036

NSO 7: -0.042

Figure S5. NSOs for the Er^{III} determined along the directions **1** (top) and **2** (bottom) corresponding to the orientation of the magnetization plane. One Er^{III} has been replaced by a Lu^{III} ion. The isosurfaces are **not** weighted by the corresponding occupation, which is indicated below each plot.

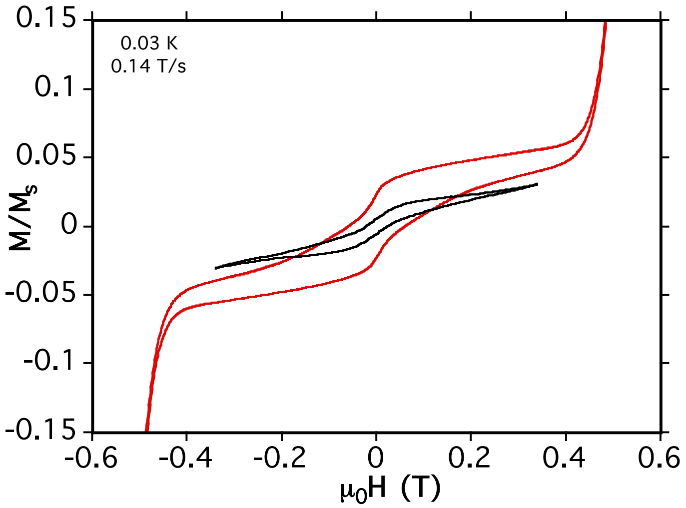

Figure S6. $M/M_S = f(\mu_0 H)$ at T = 0.03 K when the magnetic field is ramped above (red curve) and below (black curve) the critical field of 0.51 T.

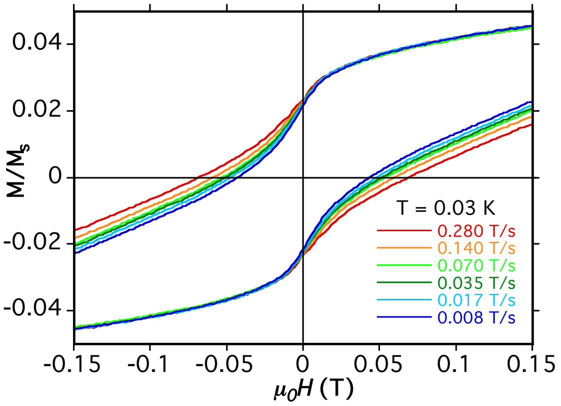

Figure S7. $M/M_S = f(\mu_0 H)$ at T = 0.03 K measured at different sweep rates showing the dependence of the width of the loop with the sweep rate for complex **3**.

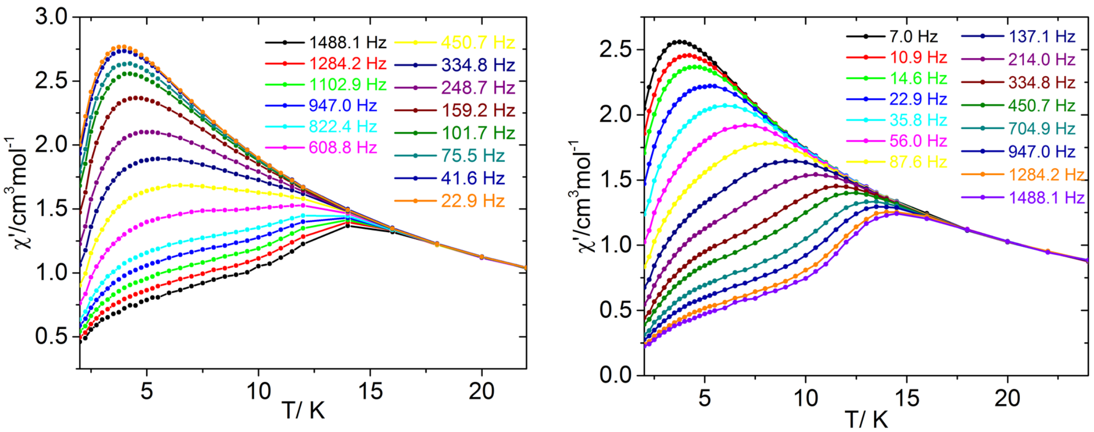

Figure S8. Temperature-dependence of the in-phase ac magnetic susceptibility for **3** under (left) zero applied dc field and (right) 2000 Oe applied dc field.

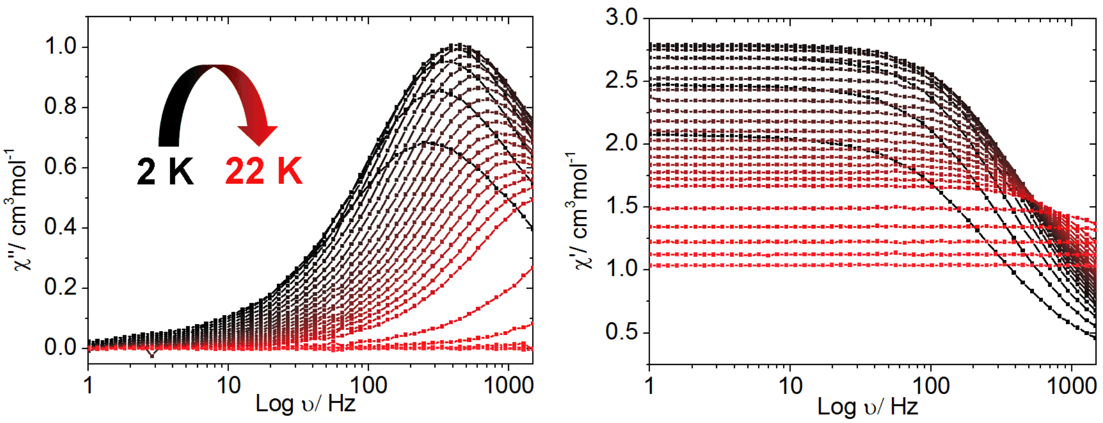

Figure S9. Frequency dependence out-of-phase (left) and in-phase (right) ac magnetic susceptibility for **3** under zero applied dc field.

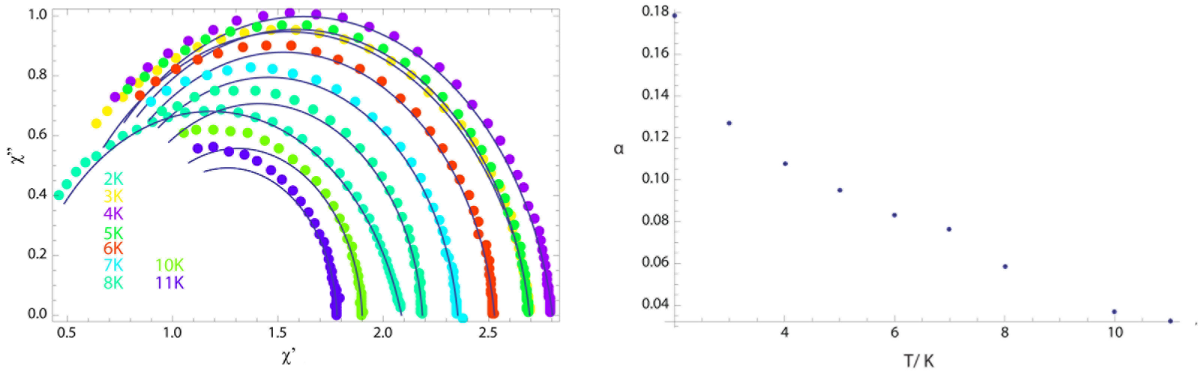

Figure S10. Cole-Cole plots for **3** under zero applied dc field. (left) Data from 2 to 11 K with fits (blue lines) obtained from the Debye equation. (right) Plot of α parameter *vs.* temperature.

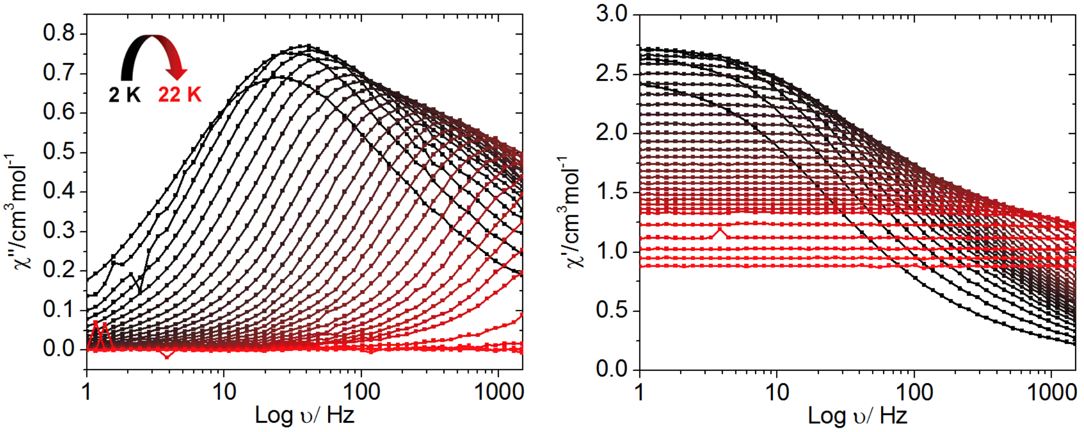

Figure S11. Frequency dependence out-of-phase (left) and in-phase (right) ac magnetic susceptibility for **3** under an applied dc field of 2000 Oe.

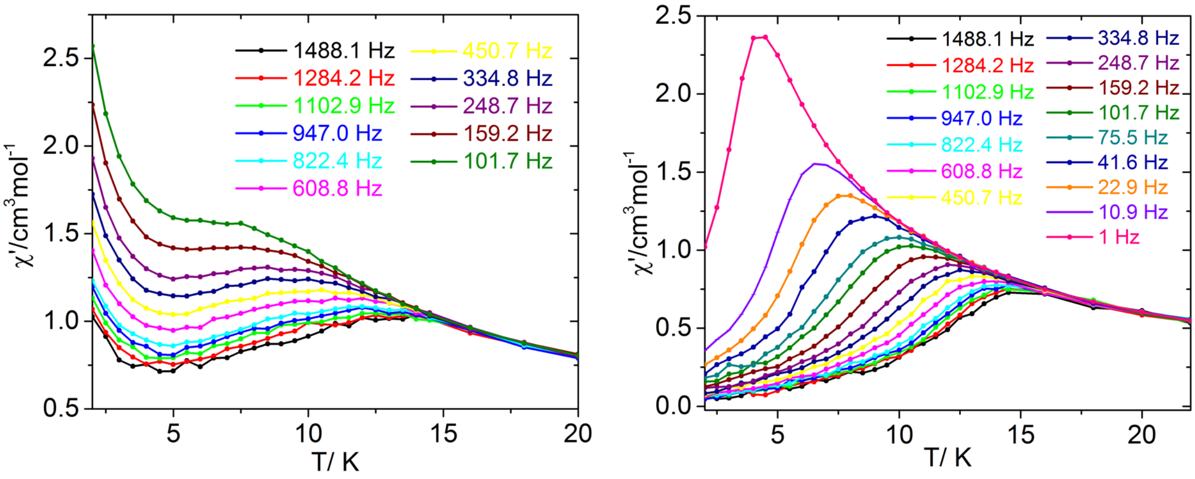

Figure S12. Temperature dependent in-phase ac magnetic susceptibility for **6** under (left) zero applied dc field and (right) 750 Oe applied dc field.

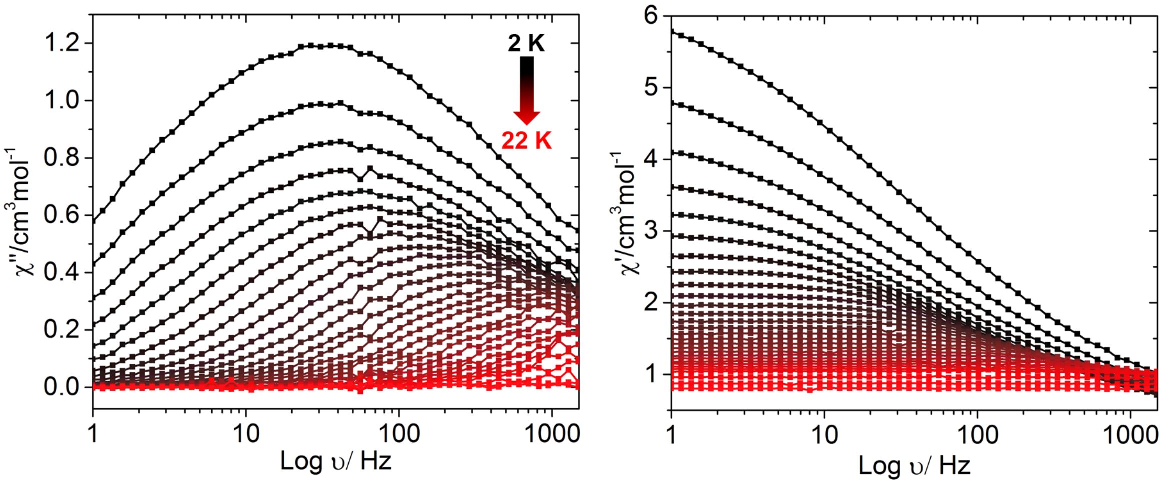

Figure S13. Frequency dependence out-of-phase (left) and in-phase (right) ac magnetic susceptibility for **6** under zero applied dc field.

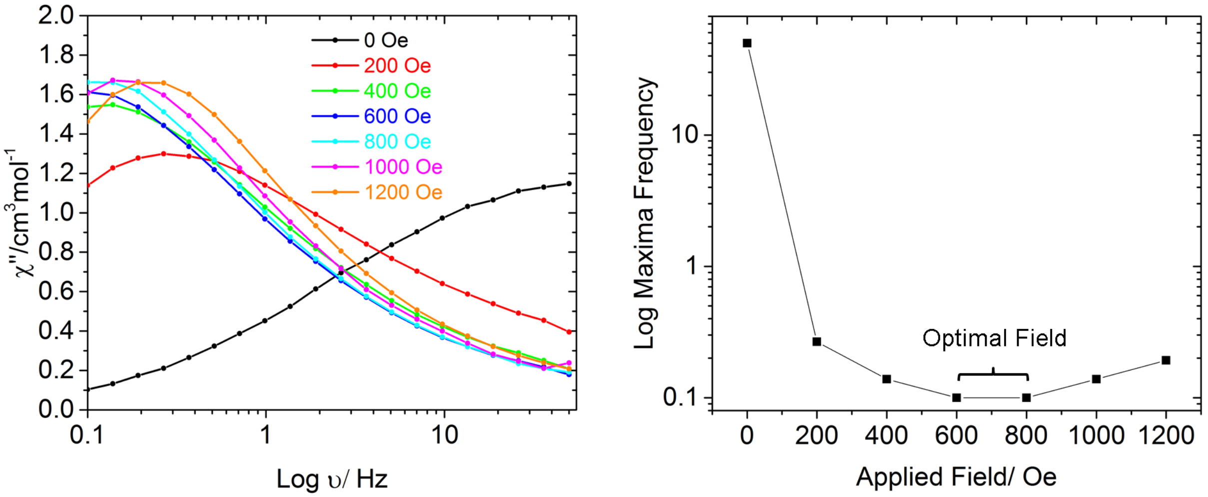

Figure S14. Field optimization of **6**. (left) Out-of-phase susceptibility measurements at 2 K at a frequency range from 1 Hz to 500 Hz at various applied fields. (right) Plot of frequency maxima *vs.* applied field.

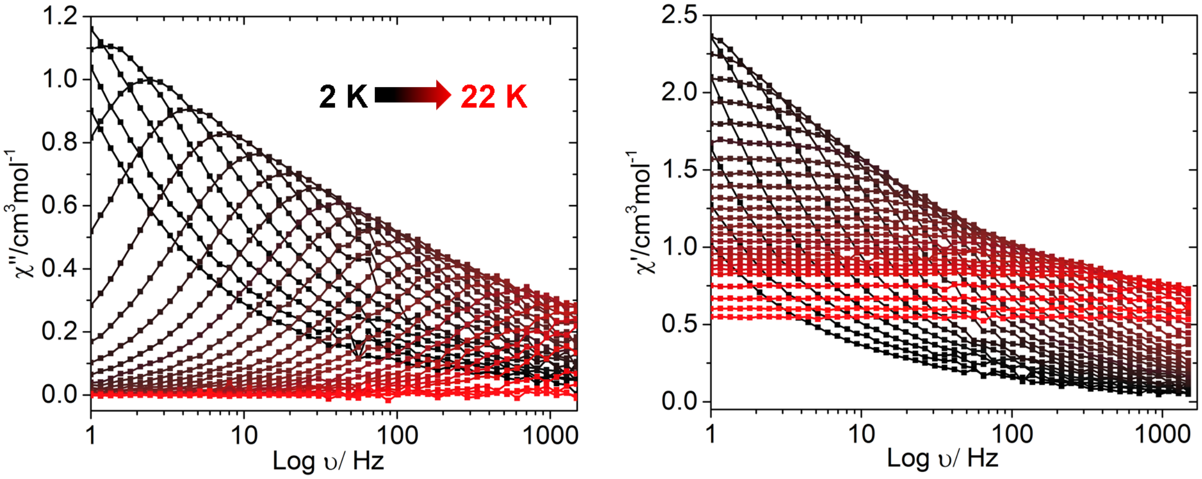

Figure S15. Frequency dependence out-of-phase (left) and in-phase (right) ac magnetic susceptibility for **6** under an applied dc field of 750 Oe.

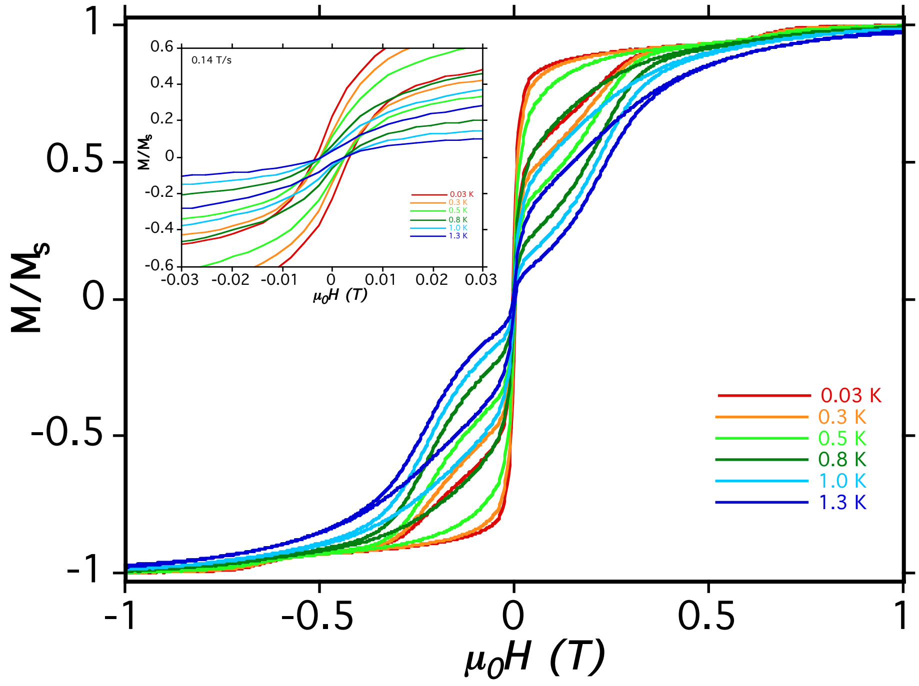

Figure S16. M/M$_S$ = f(μ_0H) at different T measured at a sweep rate of 0.14 T/s compound **6**.

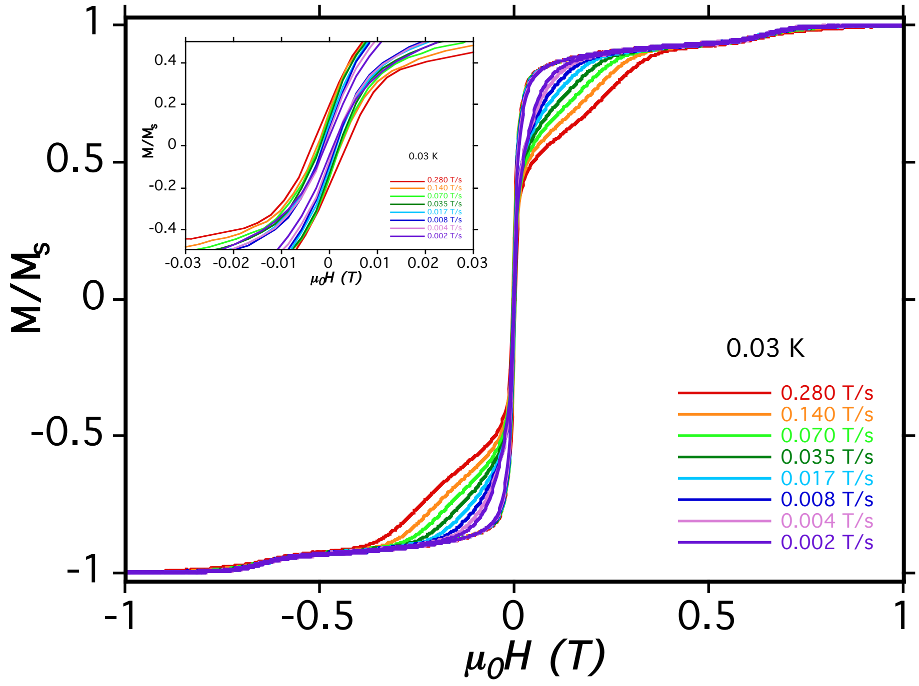

Figure S17. M/M$_S$ = f(μ_0H) at T = 0.03 K measured at different sweep rates showing the dependence of the width of the loop with the sweep rate for compound **6**.

Table S1. SHAPE[1] analysis of compound **3**.

OP (D_{8h})	HPY (C_{7v})	HPBY (D_{6h})	CU (O_h)	SAPR (D_{4d})	TDD (D_{2d})	JGBF (D_{2d})	JETBPY (D_{3h})	JBTP (C_{2v})	BTPR (C_{2v})	JSD (D_{2d})	TT (T_d)	TBPY (D_{3h})
31.549	24.076	15.088	13.16	3.463	**1.131**	11.071	27.127	3.008	2.61	2.365	13.686	24.070

Abbreviations: OP – Octagon, HPY – Heptagonal pyramid, HBPY – Hexagonal bipyramid, CU – Cube, SAPR – Square antiprism, TDD – Triangular dodecahedron, JGBF – Johnson – Gyrobifastigium, JETBPY – Johnson Elongated triangular bipyramid, JBTP – Johnson Biaugmented trigonal prism, BTPR – Biaugmented trigonal prism, JSD – Snub disphenoid, TT – Triakis tetrahedron, ETBPY – Elongated trigonal pyramid

Table S2: Energy gaps and g factors of the lowest states of $GdLuGa_4$.

Kramers Doublet	ΔE (cm^{-1})	g_i
1	0	13.92 ; 0.03 ; 0.02
2	1.0	9.64 ; 1.15 ; 0.98
3	1.6	6.07 ; 5.39 ; 4.45
4	2.1	13.10 ; 1.40 ; 0.75
5	40600	

Table S3: Energy in cm^{-1} of the states of Gd_2Ga_4 issued from the ground spin octuplet of the monomers**.** The first line with J=0 considers only dipolar interaction.

E with J=0	-0.72;-0.72;-0.62;-0.62;-0.53;-0.46;-0.46;-0.41;-0.41;-0.41;-0.41;-0.37;-0.37;-0.34;-0.34;-0.34 -0.31;-0.31;-0.22;-0.22;-0.16;-0.16;-0.15;-0.15;-0.12;-0.12;-0.09;-0.09;-0.08;-0.04; ; -0.04; 0.04;0.04;0.08;0.08;0.09;0.09;0.12;0.12;0.13;0.13;0.19;0.19;0.25;0.25;0.27;0.27;0.29; 0.29;0.30;0.40;0.40;0.40;0.40;0.43;0.43;0.45;0.50;0.57;0.57;0.58;0.58;0.75;0.75
E with J=-0.16 cm^{-1}	-2.67;-2.58;-2.58;-2.33;-2.33;-2.08;-1.92;-1.92;-1.92;-1.92;-1.62;-1.56;-1.56;-1.35;-1.35; -1.29;-1.29;-1.15;-1.02;-1.02;-0.77;-0.77;-0.64;-0.64;-0.60;-0.60;-0.53;-0.33;-0.33;-0.07;-0.07; 0.11;0.11;0.21;0.21;0.22;0.22;0.26;0.52;0.52;0.77;0.77;0.97;0.97;1.12;1.12;1.21;1.21;1.21;1.21; 1.24;1.52;1.52;1.78;1.78;2.00;2.00;2.17;2.17;2.29;2.29;2.36;2.36;2.38

Table S4: Energy gaps and g factors of the lowest Kramers doublets of $DyLuGa_4$.

Kramers Doublet	ΔE (cm^{-1})	g_i
1	0	19.47 ; 0.08 ; 0.04
2	153	15.75 ; 0.35 ; 0.66
3	241	14.09 ;1.09 ; 1.39
4	272	12.05 ; 6.15 ; 2.52
5	329	8.86 ; 4.01 ; 1.04
6	341	10.34 ; 5.68 ; 1.33

Table S5: Energy in cm^{-1} of the states of Dy_2Ga_4 issued from the ground Kramers doublet of the monomers. The first column with J = 0 considers only dipolar interaction.

states	E with J = 0	E with $J_{exc} = -0.29\ cm^{-1}$
$\vert ++\rangle \vert --\rangle$	-0.63	-2.36
$\vert +-\rangle \vert -+\rangle$	0.63	2.36

Table S6: Energy gaps and g factors of the lowest states of $TbLuGa_4$. Most of the states are close to degeneracy and form no Kramers doublets.

States	ΔE (cm^{-1})	g_i
1-2	0 ; 0.2	17.85 ; 0.00 ; 0.00
3-4	83 ; 85	16.82 ; 0.00 ; 0.00
5-6	148 ; 160	12.47 ; 0.00 ; 0.00
7-8	228 ; 240	8.80 ; 0.00 ; 0.00
9	278	
10-11	334 ; 344	16.44 ; 0.00 ; 0.00
12-13	432 ; 433	16.86 ; 0.00 ; 0.00
14-15	1828 ; 1832	

Table S7: Energy in cm^{-1} of the states of Tb_2Ga_4 issued from the ground doublet of the monomers. The first column with J=0 considers only dipolar interaction. The gap between the $|++\rangle$ and the $|--\rangle$ states is due to the small splitting in the non Kramers doublet of the monomer of 0.2 cm^{-1} (see Table S6, second line).

states	E with J=0	E with J=-0.12 cm^{-1}
$|++\rangle\,|--\rangle$	-0.63	-1.40
$|++\rangle$	0.54	1.60
$|--\rangle$	0.94	2.00

Table S8: Energy gaps and g factors of the lowest Kramers doublets of $ErLuGa_4$. (1.8 is the scaling factor applied to the energy spectrum in order to be able to fit the magnetization data)

Kramers Doublets	ΔE (cm^{-1})	ΔE*1.8 (cm^{-1})	g_i
1	0	0	9.94 ; 5.14 ; 0.25
2	19	34	7.81 ; 5.51 ; 2.13
3	50	89	12.20 ; 2.14 ; 0.40
4	77	138	8.53 ; 5.46 ; 2.43
5	139	251	8.93 ; 5.25 ; 1.94
6	192	345	11.13 ; 3.57 ; 0.84
7	235	422	9.49 ; 5.21 ; 2.84
8	278	501	15.74 ; 1.23 ; 0.58
9	6117	11010	

Table S9: Energy in cm^{-1} of the states of Er_2Ga_4 issued from the ground Kramers doublet of the monomers. The first column with J=0 considers only dipolar interaction.

states	E with J=0	E with J=2.4 cm^{-1}
$|T0\rangle = 1/\sqrt{2}\,(|+-\rangle + |-+\rangle)$	-0.20	-2.31
$|T+\rangle = 1/\sqrt{2}\,(|++\rangle + |--\rangle)$	-0.33	-1.47
$|T-\rangle = 1/\sqrt{2}\,(|++\rangle - |--\rangle)$	0.33	1.47
$|S\rangle = 1/\sqrt{2}\,(|+-\rangle - |-+\rangle)$	0.20	2.31

Table S10: Orbital and spin contributions to the g factors of the ground doublets. The ratio of the orbital and spin contributions is the same as in the free ion term. For gadolinium, the magnetic moment is the one of a pure spin. As in the free ion, the spin and orbital contributions are additive since the open shell is more than half filled and from Tb to Er, the orbital contribution increases while the spin one diminishes.

	Gd	Tb	Dy	Er
g_1	**13.92**	**17.85**	**19.47**	**9.94**
g_1^L	0.05	5.92	9.70	6.60
g_1^S	13.87	11.93	9.77	3.34
g_2	**0.03**	**0.00**	**0.08**	**5.14**
g_2^L	0.00	0.00	0.04	3.42
g_2^S	0.03	0.00	0.04	1.72
g_3	**0.02**	**0.00**	**0.04**	**0.25**
g_3^L	0.00	0.00	0.02	0.18
g_3^S	0.02	0.00	0.02	0.07

Table S11: Overlap integrals S_{AB}^{ij} of the NSOs along direction **1** of easy magnetization for the Dy_2Ga_4 complex. $S_{AB}^{ij} = \int \phi_A^i \phi_B^j d\tau$ where $\phi_{A(B)}^i$ is the NSOi centered on $Dy_{A(B)}$. The total overlap interaction is calculated as $S_{AB}^2 = \sum_{i\in A;j\in B} n_i n_j {S_{AB}^{ij}}^2$ where n_i is the population of NSOi. S_{AB}=1.0 10^{-6}.

overlap integral	NSO1$_B$	NSO2$_B$	NSO3$_B$	NSO4$_B$	NSO5$_B$	NSO6$_B$	NSO7$_B$
NSO1$_A$	-1.1 10^{-4}	-2.7 10^{-5}	-4.0 10^{-4}	-5.3 10^{-5}	-1.7 10^{-5}	1.0 10^{-4}	-9.4 10^{-5}
NSO2$_A$	-2.7 10^{-5}	-5.3 10^{-4}	6.8 10^{-4}	-6.6 10^{-5}	3.4 10^{-4}	-1.5 10^{-4}	-1.5 10^{-4}
NSO3$_A$	-4.0 10^{-5}	6.8 10^{-4}	-1.1 10^{-3}	-1.6 10^{-4}	1.6 10^{-4}	3.0 10^{-4}	1.1 10^{-4}
NSO4$_A$	-5.3 10^{-5}	-6.6 10^{-5}	-1.6 10^{-4}	4.8 10^{-4}	-2.3 10^{-4}	-2.9 10^{-5}	7.0 10^{-5}
NSO5$_A$	-1.7 10^{-5}	3.4 10^{-4}	1.6 10^{-4}	-2.3 10^{-4}	-2.4 10^{-4}	-1.3 10^{-4}	7.6 10^{-5}
NSO6$_A$	1.0 10^{-4}	-1.5 10^{-4}	3.0 10^{-4}	-2.9 10^{-5}	-1.3 10^{-4}	3.2 10^{-4}	-7.7 10^{-5}
NSO7$_A$	-9.4 10^{-5}	-1.5 10^{-4}	1.1 10^{-4}	7.0 10^{-5}	7.6 10^{-5}	-7.7 10^{-5}	2.0 10^{-4}

Table S12: Overlap integrals S_{AB}^{ij} of the NSOs along direction **1** of easy magnetization for the Tb_2Ga_4 complex. The total overlap interaction is S_{AB}^{2}=2.1 10^{-7}.

overlap integral	NSO1$_B$	NSO2$_B$	NSO3$_B$	NSO4$_B$	NSO5$_B$	NSO6$_B$	NSO7$_B$
NSO1$_A$	-1.1 10^{-4}	1.6 10^{-5}	1.4 10^{-4}	-2.3 10^{-5}	3.6 10^{-4}	1.2 10^{-4}	-8.3 10^{-5}
NSO2$_A$	1.6 10^{-5}	-3.8 10^{-4}	-5.7 10^{-5}	-1.4 10^{-4}	8.1 10^{-4}	-1.8 10^{-4}	-3.2 10^{-6}
NSO3$_A$	1.4 10^{-4}	-5.7 10^{-5}	2.3 10^{-4}	-1.8 10^{-4}	5.3 10^{-5}	9.3 10^{-5}	-8.0 10^{-5}
NSO4$_A$	-2.3 10^{-5}	-1.4 10^{-4}	-1.8 10^{-4}	-8.8 10^{-5}	-2.9 10^{-4}	-2.0 10^{-4}	3.2 10^{-4}
NSO5$_A$	3.6 10^{-4}	8.1 10^{-4}	5.3 10^{-5}	-2.9 10^{-4}	-1.0 10^{-3}	-3.1 10^{-4}	7.0 10^{-5}
NSO6$_A$	1.2 10^{-4}	-1.8 10^{-4}	9.3 10^{-5}	-2.0 10^{-4}	-3.1 10^{-4}	2.8 10^{-5}	2.1 10^{-5}
NSO7$_A$	-8.3 10^{-5}	-3.2 10^{-6}	-8.0 10^{-5}	3.2 10^{-4}	7.0 10^{-5}	2.1 10^{-5}	3.8 10^{-4}

Table S13: Overlap integrals S_{AB}^{ij} of the NSOs along directions **1** (top) and **2** (bottom) of the plane of magnetization for the Er_2Ga_4 complex. The total overlap interactions are S_{AB}^{2}=2.1 10^{-7} (top) and 5.2 10^{-7} (bottom).

overlap integral	NSO1$_B$	NSO2$_B$	NSO3$_B$	NSO4$_B$	NSO5$_B$	NSO6$_B$	NSO7$_B$
NSO1$_A$	-5.0 10^{-4}	1.1 10^{-5}	-1.9 10^{-4}	-5.1 10^{-4}	3.6 10^{-4}	9.3 10^{-5}	-1.8 10^{-4}
NSO2$_A$	1.1 10^{-5}	7.8 10^{-5}	1.4 10^{-4}	9.9 10^{-5}	8.8 10^{-5}	9.8 10^{-5}	1.8 10^{-4}
NSO3$_A$	-1.9 10^{-4}	1.4 10^{-4}	3.1 10^{-4}	2.4 10^{-4}	-2.2 10^{-4}	3.4 10^{-4}	3.6 10^{-4}
NSO4$_A$	-5.1 10^{-4}	9.9 10^{-5}	2.4 10^{-4}	-2.4 10^{-4}	6.2 10^{-4}	9.8 10^{-6}	-2.6 10^{-4}
NSO5$_A$	3.6 10^{-4}	8.8 10^{-5}	-2.2 10^{-4}	6.2 10^{-4}	2.7 10^{-4}	-1.7 10^{-4}	-8.0 10^{-5}
NSO6$_A$	9.3 10^{-5}	9.8 10^{-5}	3.4 10^{-4}	9.8 10^{-6}	-1.7 10^{-4}	3.2 10^{-4}	1.4 10^{-4}
NSO7$_A$	-1.8 10^{-4}	1.8 10^{-4}	3.6 10^{-4}	-2.6 10^{-4}	-8.0 10^{-5}	1.4 10^{-4}	3.4 10^{-4}

overlap integral	NSO1$_B$	NSO2$_B$	NSO3$_B$	NSO4$_B$	NSO5$_B$	NSO6$_B$	NSO7$_B$
NSO1$_A$	-3.7 10^{-4}	3.0 10^{-4}	-1.2 10^{-5}	-5.4 10^{-6}	-2.9 10^{-4}	1.9 10^{-5}	-7.7 10^{-5}
NSO2$_A$	3.0 10^{-4}	-1.8 10^{-4}	8.5 10^{-5}	-2.4 10^{-4}	3.6 10^{-3}	5.8 10^{-5}	4.9 10^{-7}
NSO3$_A$	-1.2 10^{-5}	8.5 10^{-5}	6.1 10^{-6}	-3.8 10^{-4}	2.8 10^{-4}	1.2 10^{-4}	-3.6 10^{-4}
NSO4$_A$	-5.4 10^{-6}	-2.4 10^{-4}	-3.8 10^{-4}	-8.9 10^{-4}	5.4 10^{-4}	2.6 10^{-4}	3.6 10^{-5}
NSO5$_A$	-2.9 10^{-4}	3.6 10^{-3}	2.8 10^{-4}	5.4 10^{-4}	4.5 10^{-4}	-3.4 10^{-5}	-1.4 10^{-4}
NSO6$_A$	1.9 10^{-5}	5.8 10^{-5}	1.2 10^{-4}	2.6 10^{-4}	-3.4 10^{-5}	1.9 10^{-4}	7.0 10^{-5}
NSO7$_A$	-7.7 10^{-5}	4.9 10^{-7}	-3.6 10^{-4}	3.6 10^{-5}	-1.4 10^{-4}	7.0 10^{-5}	2.0 10^{-4}

Calculation of the states of the dimers

Properties of the dimers are deduced from the properties of the monomers. Let us define the zero field state of the monomer A(B) as $\mid I\rangle^{A(B)}$ with the corresponding energies E$_I$. All matrix elements $\langle I|L_u|J\rangle$, $\langle I|S_u|J\rangle$ and $\langle I|M_u|J\rangle$ ($u = x, y, z$) are calculated within this basis set where $\vec{L}$, $\vec{S}$ and $\vec{M} = -\mu_B\left(\vec{L} + g_e\,\vec{S}\right)$ are the orbital, the spin angular momenta and the total magnetic momentum. g_e is the g-factor of the free electron and μ_B is the Bohr magneton. The basis set for the dimer is built as the tensor product of SO states of the monomers $\mid I\,J\rangle = \mid I\rangle^A \otimes \mid J\rangle^B$. The dipolar magnetic interaction can be written as

$$\hat{H}^{dip} = \frac{\mu_0}{4\pi R^3}\left\{\hat{\vec{M}}^A . \hat{\vec{M}}^B - 3\hat{M}_z^A\,\hat{M}_z^B\right\} \qquad (S1)$$

where R is the intermetallic distance, z the intermetallic direction and μ_0 the magnetic constant. Matrix elements for the dimers are deduced from those of the monomer as

$$\begin{aligned}\langle I\,J \,|\, \hat{H}^{dip} \,|\, I'J'\rangle = \frac{\mu_0}{4\pi R^3}\{&\langle I \mid \hat{M}_x^A \mid I' \rangle\langle J \mid \hat{M}_x^B \mid J' \rangle + \langle I \mid \hat{M}_y^A \mid I' \rangle\langle J \mid \hat{M}_y^B \mid J' \rangle \\ &- 2\,\langle I \mid \hat{M}_z^A \mid I' \rangle\langle J \mid \hat{M}_z^B \mid J' \rangle\}\end{aligned}$$

The exchange interactions are carried by the spin densities and are described by a Heisenberg-Dirac-Van Vleck (HDVV) Hamiltonian

$$\hat{H}^{Heis} = -J\,\hat{\vec{S}}^A \cdot \hat{\vec{S}}^B \qquad (S2)$$

Matrix elements of this operator are

$$\langle I\,J|\hat{H}^{heis}|I'J'\rangle = -J\{\langle I|\hat{S}_x^A|I' \rangle\langle J|\hat{S}_x^B|J' \rangle + \langle I|\hat{S}_y^A|I' \rangle\langle J|\hat{S}_y^B|J' \rangle + \langle I \mid \hat{S}_z^A \mid I' \rangle\langle J \mid \hat{S}_z^B \mid J' \rangle\}.$$

Finally, the Zeeman interaction in the dimer is described by the following Hamiltonian

$$\hat{H}^{Zee} = -\mu_B\,\vec{B} \cdot \left(\hat{\vec{M}}^A + \hat{\vec{M}}^B\right) \qquad (S3)$$

where μ_B is the Bohr magneton and $\vec{B}$ is the external magnetic field with components B_x, B_y and B_z. The matrix elements of this Hamiltonian are

$$\begin{aligned}\langle I\,J|\hat{H}^{Zee}|I'J'\rangle = -\mu_B\{&B_x\left(\langle I|\hat{M}_x^A|I' \rangle\delta_{J\,J'} + \langle J|\hat{M}_x^B|J' \rangle\delta_{I\,I'}\right) + B_y\left(\langle I|\hat{M}_y^A|I' \rangle\delta_{J\,J'} + \langle J|\hat{M}_y^B|J' \rangle\delta_{I\,I'}\right) \\ &+ B_z\left(\langle I|\hat{M}_z^A|I' \rangle\delta_{J\,J'} + \langle J|\hat{M}_z^B|J' \rangle\delta_{I\,I'}\right)\}\end{aligned}$$

where δ denotes the Kronecker symbol. Finally, the full matrix diagonalization of the total Hamiltonian $\hat{H} = \hat{H}^A + \hat{H}^B + \hat{H}^{dip} + \hat{H}^{Heis} + \hat{H}^{Zee}$ provides all energy eigenvalues and eigenvectors. This allows the calculation of the magnetization of the dimer using a Boltzmann statistics. All terms are first principles except the exchange coupling parameter J.

Magnetic dipole interaction between two magnetic planes

The magnetic plane is denoted xy and the intermetallic axis is $\vec{u} = \alpha\overrightarrow{e_x} + \beta\overrightarrow{e_y} + \gamma\overrightarrow{e_z}$. We note $\kappa = \frac{\mu_0}{4\pi R^3}$. We restrict the discussion to the lowest doublet where $|+\rangle$ and $|-\rangle$ are the local states on one monomer. The matrices for the magnetization on one center are

$$\begin{array}{ccc} \hat{M}_x & |+\rangle & |-\rangle \\ \langle +| & 0 & m \\ \langle -| & m & 0 \end{array} \qquad \begin{array}{ccc} \hat{M}_y & |+\rangle & |-\rangle \\ \langle +| & 0 & -i\,m \\ \langle -| & i\,m & 0 \end{array}$$

The states for the dimer are obtained as a tensor product of the states of the monomer $|++\rangle$, $|+-\rangle$, $|-+\rangle$ and $|--\rangle$. The matrix of operator $\hat{H}^{dip}$ defined in Eq. S1 is

$$\begin{array}{ccccc} \hat{H}^{dip} & |++\rangle & |+-\rangle & |-+\rangle & |--\rangle \\ \langle ++| & 0 & 0 & 0 & -3\kappa m^2(\alpha - i\beta)^2 \\ \langle +-| & 0 & 0 & \kappa m^2(2-3(\alpha^2+\beta^2)) & 0 \\ \langle -+| & 0 & \kappa m^2(2-3(\alpha^2+\beta^2)) & 0 & 0 \\ \langle --| & -3\kappa m^2(\alpha - i\beta)^2 & 0 & 0 & 0 \end{array}$$

In the case where **the magnetic plane is perpendicular to the intermetallic axis**, $\gamma = 1$ and $\alpha = \beta = 0$. Introducing a new basis set, $|T+\rangle = 1/\sqrt{2}\left(|++\rangle + |--\rangle\right)$, $|T-\rangle = 1/\sqrt{2}\left(|++\rangle - |--\rangle\right)$, $|T0\rangle = 1/\sqrt{2}\left(|+-\rangle + |-+\rangle\right)$, $|S\rangle = 1/\sqrt{2}\left(|+-\rangle - |-+\rangle\right)$ the previous matrix becomes

$$\begin{array}{ccccc} \hat{H}^{dip} & |T+\rangle & |T0\rangle & |T-\rangle & |S\rangle \\ \langle T+| & 0 & 0 & 0 & 0 \\ \langle T0| & 0 & 2\kappa m^2 & 0 & 0 \\ \langle T-| & 0 & 0 & 0 & 0 \\ \langle S| & 0 & 0 & 0 & -2\kappa m^2 \end{array}$$

The ground state is the $|S\rangle$ state.

In the case were **the magnetic plane includes the intermetallic axis**, $\alpha = 1$ and $\beta = \gamma = 0$ and the matrix becomes

$$\begin{array}{ccccc} \hat{H}^{dip} & |T+\rangle & |T0\rangle & |T-\rangle & |S\rangle \\ \langle T+| & -3\kappa m^2 & 0 & 0 & 0 \\ \langle T0| & 0 & -\kappa m^2 & 0 & 0 \\ \langle T-| & 0 & 0 & 3\kappa m^2 & 0 \\ \langle S| & 0 & 0 & 0 & \kappa m^2 \end{array}$$

The ground state is $|T+\rangle$ as it is the case for Er_2Ga_4 without exchange interaction.

Exchange interaction between two magnetic planes

We develop the case where there is an asymmetry in the magnetic plane and for an isotropic Heisenberg Hamiltonian J. The matrices for the magnetization on one center are

$$\begin{array}{c|cc} \hat{M}_x & |+\rangle & |-\rangle \\ \langle +| & 0 & m_x \\ \langle -| & m_x & 0 \end{array} \qquad \begin{array}{c|cc} \hat{M}_y & |+\rangle & |-\rangle \\ \langle +| & 0 & -i\,m_y \\ \langle -| & i\,m_y & 0 \end{array}$$

The matrix of operator $\hat{H}^{Heis}$ defined in Eq. S2 is

$$\begin{array}{c|cccc} \hat{H}^{Heis} & |++\rangle & |+-\rangle & |-+\rangle & |--\rangle \\ \langle ++| & 0 & 0 & 0 & -J(m_x^2 - m_y^2) \\ \langle +-| & 0 & 0 & -J(m_x^2 + m_y^2) & 0 \\ \langle -+| & 0 & -J(m_x^2 + m_y^2) & 0 & 0 \\ \langle --| & -J(m_x^2 - m_y^2) & 0 & 0 & 0 \end{array}$$

or in the other basis set

$$\begin{array}{c|cccc} \hat{H}^{Heis} & |T+\rangle & |T0\rangle & |T-\rangle & |S\rangle \\ \langle T+| & J(-m_x^2 + m_y^2) & 0 & 0 & 0 \\ \langle T0| & 0 & J(-m_x^2 - m_y^2) & 0 & 0 \\ \langle T-| & 0 & 0 & J(m_x^2 - m_y^2) & 0 \\ \langle S| & 0 & 0 & 0 & J(m_x^2 + m_y^2) \end{array}$$

With a ferromagnetic coupling $J > 0$, the ground state is $|T0\rangle$. The asymmetry in the x and y directions leads to an energy gap between $|T+\rangle$ and $|T-\rangle$ states.

The Zeeman Hamiltonian of Eq. S3 couples $|T0\rangle$ with $|T+\rangle$ ($|T-\rangle$) when the magnetic field is applied along x (y).

References

1. D. Casanova, M. Llunell, P. Alemany and S. Alvarez, *Chem.-Eur. J.*, 2005, **11**, 1479.